Contrib Mineral Petrol (1994) 116:156–168

Contributions to Mineralogy and Petrology

Titanian andradite in a metapyroxenite layer from the Malenco ultramafics (Italy): implications for Ti-mobility and low oxygen fugacity

Othmar Müntener and Jörg Hermann

Institut für Mineralogie und Petrographie, ETH Zentrum, CH-8092 Zürich, Switzerland

Received December 11, 1992 / Accepted October 13, 1993

Abstract. Ti-andradite (melanite) has been found in a metapyroxenite layer in the upper part of the Malenco ultramafics (Italy), coexisting with clinochlore, diopside and magnetite. Field observations, as well as major and trace element bulk-rock composition, strongly suggest a cumulate origin for the layer. Textural relationships indicate that Ti-andradite formed during two different metamorphic stages. Under peak metamorphic conditions (400–450° C, 5 ± 2 kbar) Ti-andradite grew in an assemblage of diopside, clinochlore, magnetite and rare ilmenite and perovskite. Later, retrograde brittle deformation induced formation of veins containing the paragenesis Ti-andradite, vesuvianite, diopside, chlinochlore, magnetite and accessory perovskite. The Ti-andradite varies considerably in TiO_2 (0.11–9.62 wt%), Fe_2O_3 (14.3–30.5 wt%), Al_2O_3 (0.65–3.90 wt%), Cr_2O_3 (<0.18–0.98 wt%) and SiO_2 (32.1–36.1 wt%); this is mostly, but not entirely, due to distinct zoning. Ti-andradite contains 0.32 to 0.66 wt% H_2O as determined by infrared spectroscopy and 0.83 to 1.76 wt% FeO. The CaO shows almost no variation (34.1 ± 0.7 wt%) and Ca completely fills the dodecahedral site. Single crystal site refinements indicate that no tetrahedral Ti or Fe replaces Si. Titanium incorporation is attributed to similar degrees of substitution along the exchange vectors $Ti^{3+}Fe^{3+}_{-1}$, $Ti^{4+}Al^{IV}Al^{VI}_{-1}Si_{-1}$ and $(Fe^{2+}, Mn^{2+}, Mg^{2+})Ti^{4+}\ 2Fe^{3+}_{-1}$. The presence of mixed valence states of both Fe *and* Ti suggests a low oxygen fugacity during crystallization of Ti-andradite. Mass balance calculations indicate an isochemical origin of the first generation of Ti-andradite in the clinopyroxenite layer. Its occurrence is restricted to antigorite-free mineral assemblages containing clinochlore of $0.95 < X_{Al} < 1.1$. The hydrothermal crystallization of Ti-rich andradite in veins demonstrates Ti mobility in aqueous fluids under moderate *P-T* conditions. The zonation patterns indicate disequilibrium conditions during vein crystallization. As no fluorine-, carbonate- and phosphate-bearing minerals were found, OH^- is most probably the ligand complexing Ti.

Introduction

Occurrences of Ti-garnets are usually associated with undersaturated alkaline igneous rocks (e.g., Howie and Woolley 1968; Dowty 1971; Amthauer et al. 1977; Huggins et al. 1977b; Deer et al. 1982; Flohr and Ross 1989) and skarns (e.g., Sawaki 1988). Ti-andradite in ultramafic rocks is relatively rare and mostly associated with metarodingites (Manning and Harris 1970; Keusen 1972; Basso et al. 1981; Evans et al. 1981; Schmidt 1989). Not associated with rodingites, it has been reported from a few localities: from San Benito County, California (in blocks of serpentinized peridotite and tectonic inclusions: Howie and Woolley 1968; Isaacs 1968; Huggins et al. 1977a, b; Lager et al. 1989; Van Baalen 1993), from the Sanbagawa terrain in Central Japan (in metamorphosed wehrlites, clinopyroxenites and gabbroic rocks: Onuki et al. 1981, 1982), and from the Mid Atlantic ridge (Switzer et al. 1970; Shibata and Thompson 1986). Onuki et al. (1981, 1982) and Lager et al. (1989) have found substantial amounts of hydrogarnet component in natural Ti-andradite.

Garnets from the Val Malenco ultramafics are primarily known as demantoids, a gem variety of andradite (Amthauer et al. 1974). Val Malenco Ti-andradite was first mentioned by Sigismund (1948), and later Grammacioli (1962, 1975), Benetti (1987), Hermann (1991), Müntener (1991) and Bedognè et al. (1993) described parageneses with diopside, chlorite, vesuvianite, magnetite and perovskite.

In this study, the assemblage Ti-andradite, diopside, chlorite, vesuvianite, magnetite and perovskite found in the upper part of the Malenco ultramafics is described. Electron microprobe (EM) analyses, infrared (IR) spectroscopy, Mössbauer spectroscopy, crystal structure refinements and colorimeric measurements were done on Ti-andradite and andradite[1]. Unit cell parameters and refractive indices were determined for both. The EM

[1] We use Ti-andradite for andradite containing more than 1 wt% TiO_2

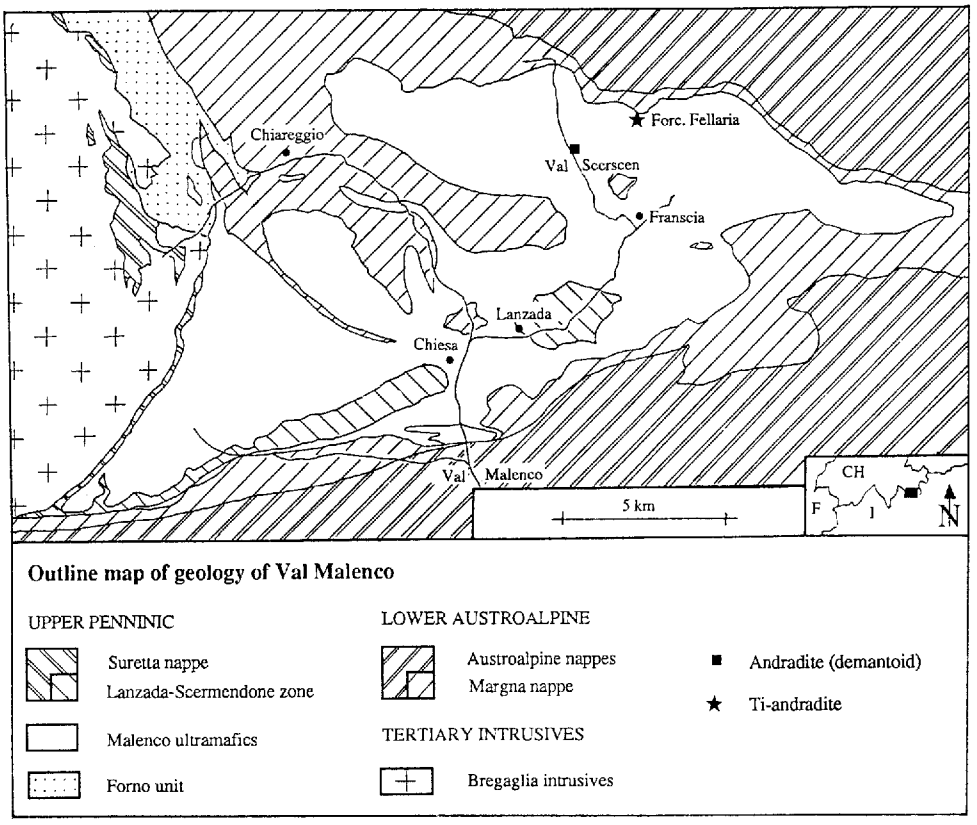

Fig. 1. Geological map of the Malenco ultramafics, partly after Montrasio (1984) and Spillmann (1993)

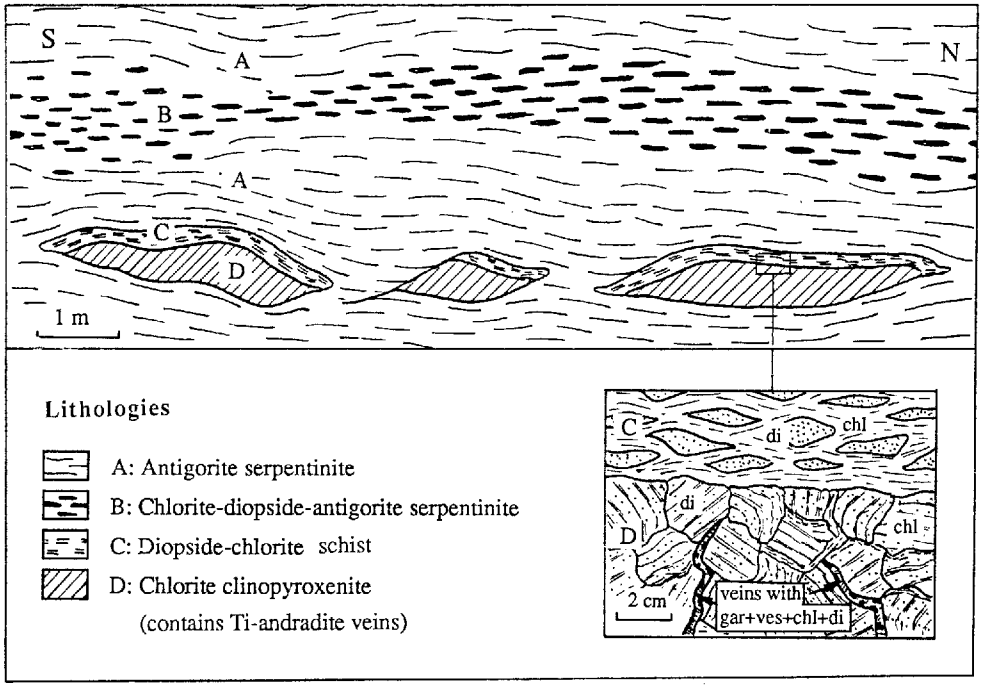

Fig. 2. Simplified sketch map of the outcrop at Forc. Fellaria. The Ti-andradite-bearing veins are located in boudinaged chlorite clinopyroxenite lenses

analyses of associated minerals as well as the whole-rock composition of the layer are presented. Mass balances and problems concerning the valence state and transport mechanisms of Ti in ultramafics are discussed.

Geological setting

The Malenco ultramafics are tectonically situated between the lower Austroalpine Margna nappe and the upper Penninic Suretta nappe (Fig. 1). They are mainly composed of metaperidotites exhibiting the assemblage diopside + antigorite + olivine + chlorite + magnetite, a product of the main Alpine upper greenschist to lower

amphibolite facies metamorphism (Trommsdorff and Evans 1974). Primary igneous layers are locally preserved, varying from harzburgite to lherzolite and olivine websterite compositions (Trommsdorff and Evans 1974; Bucher and Pfeifer 1973; Honegger 1977; Peretti 1988; this study). The samples for this study were collected from a clinopyroxenite layer near Forcella (Forc.) Fellaria (Swiss Coord. 790'870/133'800) in the northern part of Val Malenco (Fig. 1). For comparison, andradite associated with serpentine asbestos was collected in Val Scerscen (Swiss Coord. 788'600/132'730). The assemblage Ti-andradite + diopside + chlorite ± vesuvianite ± magnetite ± perovskite has been found in boudinaged lenses of chlorite-bearing clinopyroxenite (Fig. 2). The lenses are most probably relics of a primary magmatic layer. The surrounding serpentinites are highly deformed due to polyphase Alpine overprint (Hermann and Müntener 1992; see Table 2).

Near Forc. Fellaria two generations of Ti-andradite-bearing assemblages can be distinguished. During the main alpine metamorphism (400–450° C, Mellini et al. 1987; 4–7 kbar, Guntli and Liniger 1989) the first generation developed in microboudinaged old clinopyroxene, parallel to (100) and (010). The second one occurs in tension cracks which crosscut all other structures produced by ductile deformation. They were developed under retrograde conditions.

Petrography

The Ti-andradite-bearing veins are located in one outcrop near Forc. Fellaria (Fig. 1). A simplified sketch map of this outcrop is given in Fig. 2. The outcrop consists of several boudinaged lenses of chlorite-clinopyroxenite which are bordered on one side by diopside chlorite schist (C in Fig. 2). Field relations give no evidence for a reaction zone along the contact with the antigorite-rich rocks (A, B in Fig. 2).

The clinopyroxenite lenses are coarse-grained with little or no observable schistosity. Most of the minerals occur in more than one generation. The only presumably pre-metamorphic mineral is a dusty clinopyroxene with tiny inclusions of opaques. The first generation of Ti-andradite occurs within the clinopyroxenite boudins in an assemblage which is composed of poikiloblastic Ti-andradite, diopside, chlorite, opaques and rare perovskite. The most conspicuous paragenesis developed in veins crosscutting the ductile structures. The veins contain idioblastic crystals of Ti-andradite, diopside, chlorite, vesuvianite, as well as rare magnetite and perovskite.

Mineralogy of the chlorite clinopyroxenite boudins (rock D)

Garnet. The Ti-andradite of the *first generation* is usually anhedral, weakly zoned and exhibits pale brown colors in thin section. It most probably represents alteration of former exsolution lamellae of opx (orthopyroxene) and FeTi-oxides. The mostly euhedral garnets of the *second generation* occur in veins and are characterized by zonation patterns between a brown-red Ti-andradite core and a slightly yellow andradite rim (Fig. 3). The size of the garnets varies from 1 to 12 mm in diameter. Unzoned individual andradites are often translucent and of gem quality. A detailed description of the different features of the andradites is given in Table 1.

Almost all the garnets examined exhibit anomalous birefringence. Only andradite-rich garnets (And > 98%) are isotropic, whereas grossular-rich samples are strongly anisotropic. In Ti-andradite the birefringence is hardly visible because of the strong absorption color; maximum birefringence is estimated to be less than 0.007. Both biaxial positive and negative garnets occur. Birefringence in grandite garnets is likely to result from Al/Fe^{3+} ordering on the octahedral sites (Tachéuchi et al. 1982; Allen and Buseck

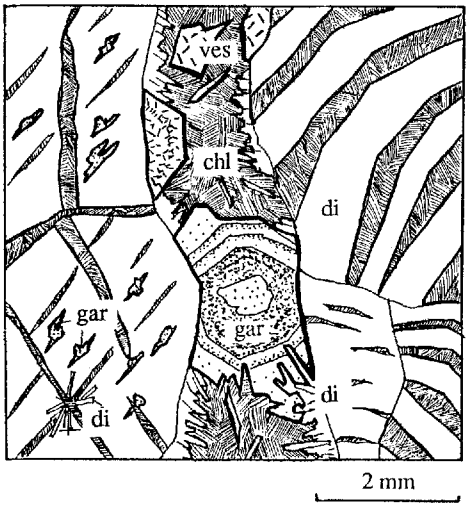

Fig. 3. Drawing from thin section showing two different Ti-andradite generations (breakdown products of primary pyroxene and vein paragenesis, respectively): Ti-andradite, *gar*; chlorite (clinochlore), *chl*; diopside, *di*; vesuvianite, *ves*

Table 1. Macroscopic and microscopic features of Val Malenco Ti-andradite and andradite (for detailed analyses see Table 3)

Sample no.	Occurrence (analysis number in brackets)	Size (mm)	Color	Color in thin section	Characteristic chemical elements
SA 10	In former pyroxene, parallel (100) and (010) (9)	0.5–1	Black to orange	Brown red to pale brown	Ti-rich (TiO_2 = 1 to 9.61 wt%)
SA 10	Vein paragenesis (core) (1–6)	2–12	Black	Dark brown red to pale brown	
SA 10	Vein paragenesis (rim) (7, 8)	1–5	Orange yellow	Slight yellow to colorless	Ti in traces (< 0.5 wt%)
SA 11	Single crystal in vein (10)		Pale yellow	Slight yellow to colorless	
SA 12	Single crystal in vein (11–13)	1–4	Emerald green	Slight green	Cr-rich (Cr_2O_3 = 1 to 4.82 wt%)
SA 17	Asbestos mine Val Scerscen (14, 15)	3–11	Pale green	Colorless	Pure andradite

Table 2. Chemical composition of the ultramafic layer and the surrounding Malenco serpentinite. The Ti-andradite veins have been found in chlorite-clinopyroxenite. Normative composition calculated with MANNOR (written by P. Ulmer) using the following conditions: Tschermaks component in pyroxene = 0.1; SAX 1, 2, 3, 5, KFX 8, $Fe^{3+}/Fe_{total} = 0.1$; SAX 4, 6, 8, $Fe^{3+}/Fe_{total} = 0.25$; SAX 7, $Fe^{3+}/Fe_{total} = 0.5$

Sample no.		A Antigorite serpentinite		B Chlorite-diopside-antigorite serpentinite	C Diopside-chlorite schist		D Chlorite-clinopyroxenite				
		KFX 8	SAX 3	SAX 5	SAX 1	SAX 2	SAX 4	SAX 6	SAX 7	SAX 8	2σ
Major elements[2] (wt%)	SiO_2	39.2	40.3	41.6	39.4	40.7	44.1	47.7	49.0	48.0	0.72
	TiO_2	0.10	0.10	0.06	0.07	0.06	0.17	0.19	0.17	0.26	0.01
	Al_2O_3	2.6	3.0	3.3	10.7	9.9	6.5	4.0	2.7	4.6	0.32
	$Fe_2O_3^1$	8.56	8.28	7.94	6.24	5.82	6.54	5.57	5.33	4.32	0.06
	MnO	0.11	0.13	0.11	0.11	0.11	0.15	0.12	0.11	0.12	0.02
	MgO	35.8	35.9	33.4	24.4	24.1	21.5	19.0	17.7	19.4	0.17
	CaO	0.7	1.6	4.3	10.4	11.4	15.4	20.7	22.7	20.1	0.16
	P_2O_5	0.04	<0.02	<0.02	0.02	0.02	0.06	<0.02	<0.02	<0.02	0.02
	Cr_2O_3	0.28	0.33	0.31	0.41	0.38	0.43	0.10	0.08	0.08	0.01
	NiO	0.28	0.29	0.22	0.16	0.17	0.10	0.08	0.05	0.06	0.01
	volatiles	10.96	10.77	9.56	8.64	6.53	4.66	2.81	1.97	2.88	
	$\sum$	98.6	100.7	100.8	100.5	99.2	99.6	100.2	99.8	99.8	
											Detection limit
Trace elements (ppm)[3]	Sr	<15	<15	<15	<15	<15	47	<15	<15	21	15
	Y	<4	<4	<4	<4	<4	<4	<4	<4	4	4
	V	47	51	60	64	52	94	90	91	128	14
	Cr	1781	2596	2659	4185	4002	4175	960	821	810	25
	Ni	1773	1848	1473	1114	1152	798	577	382	417	11
	Co	42	62	57	72	70	56	45	43	33	16
	Cu	<12	<12	<12	<12	24	<12	<12	<12	<12	12
	Zn	48	40	40	38	34	51	27	21	24	7
	Sc	9	11	10	10	6	34	41	41	48	2
	S	<100	216	<100	<100	<100	<100	<100	<100	<100	100
Normative composition (mineral %)	Cpx	3.1	6.7	18.2	44.2	48.2	64.7	84.1	90.6	81.8	
	Opx	38.9	37.3	32.9	22.9	21.5	12.9	0.8	0.0	5.2	
	Olivine	55.6	53.1	46.1	19.8	18.8	16.1	13.7	9.1	11.5	
	Spinel	2.4	2.9	2.6	13.1	11.5	6.3	1.4	0.3	1.5	
	X_{Mg}[4]	0.90	0.90	0.90	0.89	0.90	0.89	0.90	0.93	0.92	
Primary rock		Harzburgite		Lherzolite	Spinel-olivine websterite		Olivine-pyroxenite				

[1] Fe_2O_3 is total iron
[2] $Na_2O < 0.18$, K_2O not detected
[3] Zr < 10 ppm, Ba < 10 ppm, Rb < 8 ppm, Pb < 5 ppm, Th < 5 ppm, U < 10 ppm, Nb < 4 ppm, Ce < 21 ppm, La < 20 ppm, and Nd < 25 ppm
[4] $X_{Mg} = Mg/(Mg + Fe^{2+})$

1988; Kingma and Downs 1989) or from lattice mismatch at compositional, twin or grain boundaries (Kitamura et al. 1986). The lamellae inside the birefringent andradite did not have different chemical compositions and are therefore different from those described by Jamtveit (1991). In the samples studied however, there is a correlation between birefringence and grossular component (Müntener 1991). Almost pure andradite in samples from Val Scerscen (Table 1) is isotropic.

Chlorite. Chlorite of the *first generation* is widespread in metamorphosed olivine websterite and clinopyroxenite. It grew either along exsolution lamellae of former opx in primary cpx (clinopyroxene)-rich pyroxenes (Fig. 3. Fig. 4) or it formed the matrix of diopside-chlorite schists (Fig. 2, C in Table 2). Chlorite shows systematic differences in its optical properties and chemical composition (Table 6). Pale green Fe-pennine with anomalous brown or rarely blue interference color is present in olivine-websterite layers and/or coexisting with antigorite (A and B in Table 2, sample S 60 in Table 6). Colorless clinochlore with first-order grey interference color is the typical feature of the clinopyroxene and its margin (C and D in Table 2).

Second generation chlorite occurs in veins together with Ti-andradite an is of clinochlore composition as well. It is present as intergrowths with diopside (Fig. 3) and as idiomorphic single crystals (maximum size 10 mm) exhibiting weak zonation.

Diopside. Diopside of the *first generation* is dusty but almost colorless in thin section, and most probably represents the cpx-rich part of a primary pyroxene. It is up to 3 cm in size. The diopside contains considerable amounts of Cr_2O_3 (up to 0.7 wt%) and Na_2O (up to 0.6 wt%) and minor quantities of Al_2O_3 (up to 0.4 wt%), TiO_2 (up to 0.3 wt%), and of MnO and NiO (around 0.1 wt%) as well as tiny inclusions of opaques.

The *second generation* occurs as fine and clear needles in Ti-andradite bearing veins (maximum size 1 cm) or as xenomorphic intergrowths with chlorite (Fig. 3). This diopside is almost pure $CaMgSi_2O_6$ with minor amounts of hedenbergite component (< 5 mol%).

Vesuvianite. Vesuvianite is closely associated with chlorite, diopside and garnet (Fig. 3) and occurs *only* as part of the vein assemblage. Both anomalous blue-brown and normal interference colors are

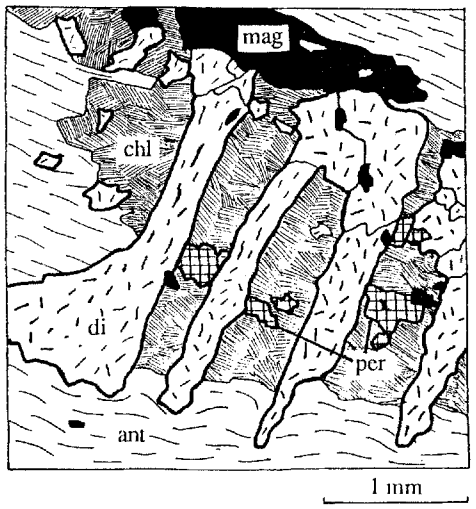

Fig. 4. Drawing from thin section showing the paragenesis diopside, *di*; chlorite (Fe-pennine), *chl*; magnetite, *mag*; and perovskite, *per*, as breakdown products of primary pyroxene, embedded in an antigorite, *ant*, matrix

present. Most of the vesuvianite is colorless in thin section but in a few samples patches of a red-brown tint are recognizable. Vesuvianite varies considerably in composition (Al_2O_3: 12.02 to 17.56 wt%; FeO 2.58 to 7.26 wt%) and contains significant amounts of TiO_2 (0.18 to 5.13 wt%). Ti-vesuvianite with a similarly high concentration of TiO_2 has rarely been reported in literature. Myasnikov (1940) described Ti-vesuvianite associated with perovskite. The crystal chemistry of Ti-vesuvianite has been investigated by Manning (1975) and Manning and Tricker (1975). Murdoch and Ingram (1966) found a REE-titanian vesuvianite together with Ti-andradite, perovskite, diopside and chlorite in veins similar to those from Forc. Fellaria.

Accessories. Accessory minerals occurring either in dusty diopside or in veins are magnetite, perovskite, ilmenite, pentlandite and hematite. *Magnetite* is common in the surrounding serpentinite. In the clinopyroxenite it occurs as aggregates of up to 1 cm in size associated with clinochlore, diopside and pentlandite. The second generation occurs as single crystals in veins exhibiting octahedral or rhombododecahedral shape. Its composition is close to pure magnetite. In thin section *perovskite* can be observed in chlorite lamellae between diopside (Fig. 4), where it is brown to almost opaque depending on the size (maximum size 0.5 mm). In veins perovskite rarely occurs as single crystals associated with chlorite. It contains small amounts of FeO and MnO (<0.5 wt%): *Ilmenite* and *hematite* occur as tiny inclusions in dusty diopsides.

Analytical procedure

Mineral compositions were analyzed using a Cameca SX-50 microprobe, equipped with five crystal spectrometers. Samples were coated with 200 Å of carbon. Operating parameters include an acceleration potential of 15 kV, a beam current of 20 nA and a beam size of ~1 mm. The data time was 20 s for chlorites and 10 s for all other minerals. Data collection background positions on both sides of the peaks was half the time of data collection on the respective peak position. A natural andradite was used as standard for Ca and Fe, and was carefully checked against another natural standard for its composition. For other elements natural and synthetic oxides and silicates were used. Raw data were corrected for drift, dead time and background. A ZAF-type correction procedure was applied to the data (Pouchon and Pichoir 1984). The relative error due to counting statistics (2σ) is listed in Tables 3 and 4. The bulk chemical composition of the ultramafic layering was determined by X-ray fluorescence (XRF) analyses, with a sequential spectrometer (Philips PW 1404) using natural USGS reference rock samples for calibration. Rocks were ground in a tungsten carbide mill. Major elements were determined using glass beads which were fused from ignited (at 1050° C) rock powders mixed with $Li_2B_4O_7$ in a 1/5 ratio (Dietrich et al. 1976) in gold platinum pans at 1150° C. The intensities were corrected for instrumental drift, background and matrix effects. Trace elements were determined by XRF analyses of 10 g powder samples using the synthetic background method for which major elements have to be known (Nisbet et al. 1979). The relative error (2σ) due to counting statistics and regression, and detection limits are listed in Table 2.

The refractive index was determined by using the immersion method (grain size 75–150 mm, monochromatized light of 589 nm). The calibration of the standard solutions ('Cargille Index of refractive liquids') was checked with a Leitz-Jelley refractometer.

The water content of carefully separated single grains of Ti-andradite and andradite (SA 10) was determined by Leco IR spectroscopy (Leco RC 412) using Donham gypsum rock C as standard material. After drying the powdered samples at 105° C for 24 h the garnets were gradually heated under oxygen atmosphere in a quartz oven from 100 to 1100° C. The released vapor phase was simultaneously recorded by infrared cells. The resulting accuracy for H_2O is ±3% relative to the result or ±0.10 of the absolute value.

Bulk-rock chemistry

The bulk composition of the different samples (A–D in Table 2) as well as calculated primary mineral assemblages using a "spinel peridotite" norm[2] are given in Table 2. The rocks (A) and (B) exhibit a typical ultrabasic composition compared to ordinary Alpine metaperidotites. Depending on the amount of CaO the composition is either harzburgitic (A) or lherzolitic (B). The normative mineral assemblage yields for (C) an olivine-spinel websterite, and for (D) an olivine clinopyroxenite. The high Cr and Ni content and the high X_{Mg} [Mg/(Mg+Fe^{2+}) 0.89 to 0.92] confirm the field observations that they are all part of a layered ultramafic body. Normative spinel ranges from 0.3 to 13.1%. The rocks with high normative spinel exhibit high Cr contents which might be due to Al replacement by Cr in spinel.

Garnet and vesuvianite in ultramafic environments are often associated with rodingites which are metasomatically altered basalts, gabbros or tectonic inclusions of sediments (e.g., Rice 1983). Compared with published analyses of metarodingites (e.g., Evans et al. 1979, 1981), the analyzed chlorite clinopyroxenite contains significantly lower V, MgO, Al_2O_3, and TiO_2, and higher Cr and Ni than usual metarodingites. For these several reasons we conclude that the garnet-bearing rocks represent a former pyroxenite layer and are not a product of rodingitization.

The normative composition of the rocks is displayed graphically in Fig. 5, where they are compared with analyses described by Trommsdorff and Evans (1974), Bucher and Pfeifer (1973) and Peretti (1988). This comparison demonstrates several features: Serpentinites of lherzolitic or harzburgitic composition (A and B in Ta-

[2] Spinel peridotite norm: corundum and anorthite were converted to spinel, opx and cpx using a computer program (MANNOR) written by P. Ulmer

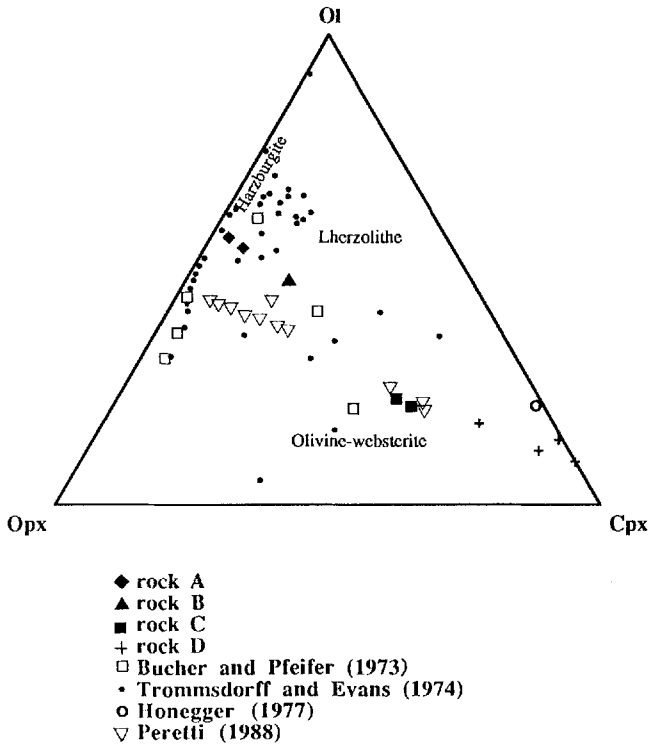

Fig. 5. Normative olivine, orthopyroxene and clinopyroxene in ultramafic rocks from the Central Alps. Normative conditions are given in Table 2

ble 2) are widespread in the Malenco ultramafics and in other peridotites from the Alps. The diopside-chlorite schist (C) is comparable with the Cpx-richest part of a magmatic layer described by Peretti (1988). His analyses show Al_2O_3 contents of only about 5 wt% as compared to about 10 wt% in rock C (Table 2). Chlorite clinopyroxenite (D) has rarely been described in peridotites from the Alps and is mentioned by Honegger (1977) from the Malenco ultramafics.

The Ti-andradite-bearing veins lie therefore in a layer whose chemical composition is very different from the major part of the Malenco ultramafic body.

Composition of andradite

Compositional variation in andradite

The chemical composition of the Val Malenco andradite was mainly determined by means of *EM analyses*. It contains only small concentrations of MnO and MgO (Table 3). Wavelength spectra did not reveal detectable amounts of Co, Cu, Zn, Ni, Nb, Na, K, Zr, V or F. Recalculation of EM analyses as well as site refinements further indicated that the dodecahedral site is completely occupied by Ca (Table 3). Thus, the Val Malenco andradite can be described as Ca-garnet with compositional variation only at the octahedral and tetrahedral sites.

Table 3. Representative microprobe analyses of Val Malenco andradite: (1–9, sample SA 10; 10, sample SA 11; 11–13, sample SA 12; 14, 15, sample SA 17). Sample description see Table 1

Wt%	Sample				SA 10					SA 11	SA 12			SA 17		Average relative error (2σ) in %
	Analysis															
	1	2	3	4	5	6	7	8	9	10	11	12	13	14	15	
SiO_2	33.9	33.0	33.2	33.3	34.1	32.9	35.7	35.7	34.5	35.3	34.9	35.2	35.3	34.6	34.7	1.0
TiO_2	6.49	9.62	8.57	8.24	3.92	8.65	0.53	0.25	3.24	0.24	1.14	0.61	0.58	<0.10	<0.10	6.0 (at 0.5% level) 2.4 (at 5.0% level)
Cr_2O_3	0.36	<0.18	<0.17	<0.18	<0.18	0.31	<0.17	<0.18	1.73	<0.18	4.82	2.87	3.61	<0.18	<0.18	6.6 (at 0.4% level) 3.0 (at 4.0% level)
Al_2O_3	2.97	2.05	1.34	1.52	1.72	2.37	3.89	2.31	0.93	1.40	0.76	0.73	0.72	<0.15	<0.15	6.0 (at 0.3% level) 2.6 (at 3.0% level)
Fe_2O_3	17.3	15.4	17.4	18.2	23.8	16.0	25.8	27.6	24.0	29.9	23.8	26.7	25.6	31.2	31.4	2.4
FeO[1]	2.47	3.56	3.96	3.07	0.92	3.30	0.00	0.00	0.45	0.00	0.00	0.00	0.00	0.00	0.00	
MnO	0.19	0.25	0.21	<0.18	<0.18	<0.18	<0.17	<0.18	<0.18	<0.18	<0.18	<0.18	<0.18	<0.18	<0.18	6.8
MgO	<0.18	<0.17	<0.18	<0.18	<0.17	<0.17	<0.17	<0.17	<0.18	<0.18	<0.18	<0.17	<0.17	0.18	<0.18	6.4
CaO	34.1	34.4	33.7	34.2	33.8	34.1	34.3	33.8	33.9	33.8	33.7	33.7	33.5	33.4	33.0	1.2
$\sum$	97.8	98.3	98.4	98.5	98.3	97.6	100.2	99.7	98.8	100.6	99.3	99.8	99.3	99.2	99.1	
Ions calculated on the basis of 8 cations																
Si	2.87	2.79	2.82	2.82	2.90	2.81	2.95	2.99	2.93	2.94	2.95	2.96	2.98	2.94	2.96	
Ti	0.41	0.61	0.55	0.52	0.25	0.55	0.03	0.02	0.21	0.02	0.07	0.04	0.04	0.00	0.00	
Cr	0.02	0.00	0.00	0.00	0.00	0.02	0.00	0.00	0.12	0.00	0.32	0.19	0.24	0.00	0.00	
Al	0.30	0.21	0.14	0.15	0.17	0.24	0.38	0.23	0.09	0.14	0.08	0.07	0.07	0.00	0.00	
Fe^{3+}	1.10	0.98	1.12	1.16	1.52	1.03	1.60	1.73	1.53	1.88	1.51	1.67	1.63	1.99	2.02	
Fe^{2+} [1]	0.18	0.25	0.28	0.22	0.07	0.23	0.00	0.00	0.03	0.00	0.00	0.00	0.00	0.00	0.00	
Mn	0.01	0.02	0.02	0.01	0.00	0.00	0.00	0.00	0.00	0.00	0.00	0.00	0.00	0.00	0.00	
Mg	0.00	0.00	0.00	0.00	0.00	0.00	0.00	0.00	0.00	0.00	0.00	0.00	0.00	0.01	0.00	
Ca	3.10	3.12	3.07	3.10	3.08	3.11	3.03	3.03	3.08	3.03	3.05	3.04	3.03	3.04	3.02	

[1] Calculated assuming stoichiometry

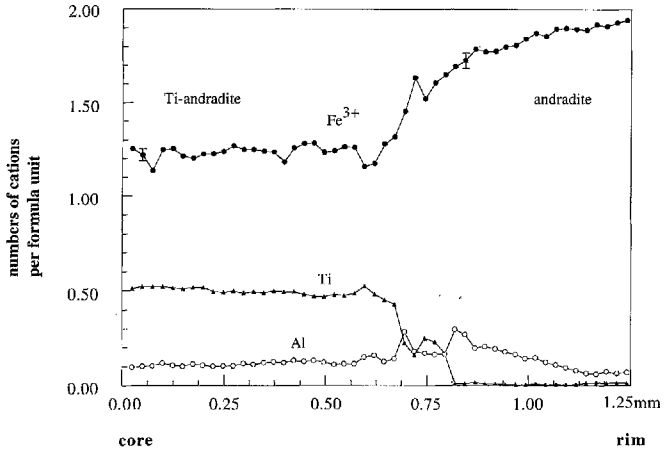

Fig. 6. Variation of the octahedrally coorinated major elements through a Ti-andradite of sample 13. Ti, *filled triangles*; Al, *open circles*; and Fe^{3+}, *dots*. Error *bars* represent the relative error due to counting statistics (2σ). Error bars for Al and Ti are *smaller* than symbols

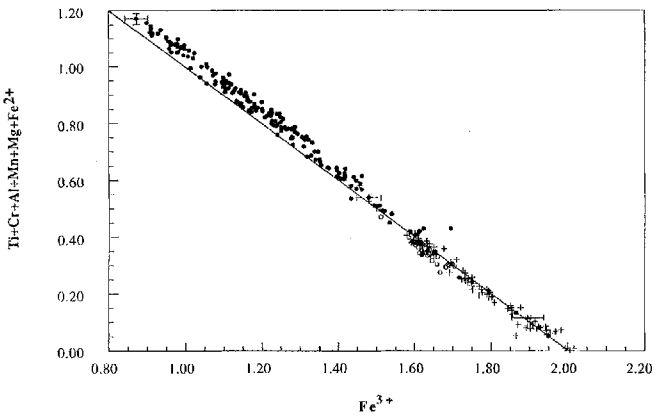

Fig. 7. Octahedral cation exchange in andradite from Val Malenco, based on electron microprobe analyses. The diagram shows the substitution of Ti, Al, Cr and Fe^{2+} for Fe^{3+}. Slope of the theoretical line of exchange is -1. Note the positive deviation from the theoretical line for garnets with Ti as main substitute for Fe. This is mostly due to significant hydrogarnet component (see text for discussion). Error *bars* represent the relative error due to counting statistics (2σ). *Filled circles*, Ti is the main substitute for Fe; *open circles*, Cr is the main substitute for Fe; *crosses*, Al is the main substitute for Fe

Representative analyses (Table 3) exhibit a variation in Cr, Al, Fe, Ti and Si. Ti-andradite is characterized by Si deficiency (SiO_2: 32.9 to 34.9 wt%) which is not uncommon for Ti-garnets in ultramafics (eg., Zedlitz 1933; Howie and Woolley 1968; Basso et al. 1981; Onuki et al. 1981, 1982; Lager et al. 1989). The cores of andradite from sample SA 10 are always enriched in Ti (TiO_2: 5.55 to 9.62 wt%) and they show a narrow transition to the Ti-poor rims (Fig. 6). In contrast to andradite, Ca in Ti-andradite significantly exceeds 3.00 per formula unit[3]. These observations as well as the lower analysis totals in Ti-rich garnets (Table 2) suggest presence of additional elements in Ti-andradite which were either not analyzed or not detectable by microprobe.

Based on the constraints described above the compositional variation of Val Malenco andradite involves mainly the octahedral site. This is demonstrated by Fig. 7. Within the limits of analytical error Fe^{3+} and $\sum$ Al+Cr+Ti+Mn+Mg+Fe^{2+} correlate negatively along a theoretical line of slope -1 (Fig. 7). During this exchange CaO remains almost constant (CaO: 34.1 $\pm$ 0.7 wt%). Compositional variation in andradite (i.e., Cr and Al are the primary substitutes for Fe^{3+}) is ascribed to the simple exchange vectors $AlFe_{-1}$ and $CrFe_{-1}$. In analyses where Ti is the primary substitute for Fe, a positive deviation from the theoretical line (i.e., $\sum$ y-cations = 2) can be found, but this is due to cation normalization based on H_2O-free EM analyses and small amounts of Al^{IV} (see above and Table 5).

IR spectroscopy for H_2O was made on carefully separated Ti-andradite cores and andradite rims from sample SA 10. IR-spectroscopy revealed that the Ti-andradite contains 0.66 ($\pm$0.10) wt% H_2O which is is in good agreement with water contents derived from site refinements (Table 4). The andradite rim contains only 0.32 ($\pm$0.10) wt% H_2O (Table 5).

The results of the *site refinements* (unit-cell, oxygen parameters, interatomic distances and water content, respectively) between the Ti-rich core and the andradite rim are compared in Table 4. The slightly larger tetrahedral T–O and dodecahedral X1-O, X2-O distances of the Ti-andradite relative to that of andradite is consistent with an increase in the unit-cell parameter. How-

Table 4. Unit-cell parameters (Å), oxygen parameters, interatomic distances (Å) and comparison of water contents (wt%) for Val Malenco andradite

	Sample SA 12	
	Ti-andradite (core)	Andradite (rim)
Unit-cell	12.089 ($\pm$0.002)	12.050 ($\pm$0.002)
Oxygen parameters		
x	0.03894 ($\pm$0.00008)	0.03935 ($\pm$0.00008)
y	0.04810 ($\pm$0.00009)	0.04828 ($\pm$0.00009)
z	0.65466 ($\pm$0.00009)	0.65521 ($\pm$0.00009)
Interatomic distances		
T–O	1.658 ($\pm$0.001)	1.646 ($\pm$0.001)
Y–O	2.014 ($\pm$0.001)	2.015 ($\pm$0.001)
X1–O	2.365 ($\pm$0.001)	2.359 ($\pm$0.001)
X2–O	2.512 ($\pm$0.001)	2.503 ($\pm$0.001)
Water content		
X-ray refinement	0.9	0
IR-spectroscopy	0.66	0.32

[3] Ca in excess of 3.00 cations is not uncommon for melanite in ultramafics (Huggins et al. 1977b; Onuki et al. 1981; Lager et al. 1989), but it is striking that most of these melanites contain significant hydrogarnet component. Therefore excess Ca is most probably an artifact of a water free cation normalization. Huggins et al. (1977b) did not find hydrogarnet component. In this study however, despite allowance for H_2O Ti-andradite still contains a significant Ca excess

Table 5. Crystal chemical formula and refractive index of Val Malenco Ti-andradite (sample SA 10). The water content has been calculated as hydrogarnet component $(SiO4)^{4-}$ $(OH_4)^{-}_{1}$. See text for discussion

Wt%	Andradite[1]		Ti-andradite (melanite)[1]		Ti-andradite (melanite)[2]	
	Mean $n=35$	Standard deviation (2σ)	Mean $n=94$	Standard deviation (2σ)	Mean $n=94$	Standard deviation (2σ)
SiO_2	35.4	0.4	33.3	0.4	33.3	0.4
TiO_2	0.16	0.07	4.93	1.12[3]	4.26	1.12[3]
Ti_2O_3			2.43		3.04	
Cr_2O_3	trace		0.35	0.29	0.35	0.29
Al_2O_3	1.77	0.71	1.59	0.77	1.59	0.77
Fe_2O_3	27.7	1.1	19.4	2.0	20.3	2.0
FeO	0.83		1.76		0.96	
MnO	trace		0.17	0.04	0.17	0.04
MgO	trace		trace		trace	
CaO	33.8	0.3	34.1	0.3	34.1	0.3
H_2O	0.32		0.66		0.66	
$\sum$	100.1		98.7		98.7	
Ions calculated on the basis of 8 cations						
Tetrahedral cations						
Si	2.95		2.80		2.80	
(H_4)	0.04		0.09		0.09	
Al^{IV}	0.01		0.11		0.11	
Octahedral cations						
Ti^{4+}	0.01		0.31		0.27	
Ti^{3+}	–		0.17		0.21	
Cr	0.00		0.02		0.02	
Al	0.16		0.06		0.06	
Fe^{3+}	1.74		1.24		1.29	
Fe^{2+}	0.06		0.12		0.07	
Mn	0.01		0.01		0.01	
Mg	0.00		0.00		0.00	
Ca	0.02		0.07		0.07	
Dodecahedral cations						
Ca	3.00		3.00		3.00	
Ti exchange vectors						
$Al^{IV}Ti^{4+}(Al^{VI}Si)_{-1}$			23%		23%	
$Ti^{3+}Fe^{3+}_{-1}$			35%		43%	
$Me^{2+}Ti^{4+}2Fe^{3+}_{-1}$	100%		42%		34%	
Refractive index (n)	1.848	±0.003	1.878	±0.002		

[1] Formula calculated on the basis of EM analyses, site refinements, colorimetry and infrared spectroscopy. Fe_2O_3 was calculated as 1.1113 ($FeO_{total} - FeO_{color}$)
[2] Formula calculated on the basis of EM analyses, site refinements, Mössbauer spectroscopy and IR spectroscopy. Fe_2O_3 was calculated as 1.1113 ($FeO_{total} - FeO_{Möss}$)
[3] Standard deviation calculated for total TiO_2

ever, the site refinements for the tetrahedral position indicate neither tetrahedral Fe nor Ti, in agreement with the low scattering power observed at the tetrahedral site. Therefore it is likely that hydrogarnet component (O_4H_4) $(SiO_4)_{-1}$ substitutes the Si deficiency in Ti-andradite (minor Al can not completely be excluded because of the similar atomic numbers of Al and Si). The site refinement parameters for Ti-andradite are in good agreement with the published data of Lager et al. (1989). In contrast, site refinements of a synthetic Ti-garnet (Weber et al. 1975) indicate considerable amounts of tetrahedral Fe and Ti, resulting in a much larger unit cell (a = 12,2399 Å) and a larger T–O distance (T–O = 1,744 Å). The site refinement data of the andradite rim correspond well with natural and synthetic andradite (eg., Amthauer et al. 1974; Kingma and Downs 1989; Armbruster and Geiger 1993).

Colorimetric measurements were made in order to determine the "FeO"[4] content in Ti-andradite and andradite. For the Ti-andradite "FeO" = 1.76 (±0.12) wt% resulting in a $X_{Fe} = 0.08$ (±0.01)[5]. The measured "FeO" for andradite is 0.83 (±0.12) wt% resulting in a $X_{Fe} =$

[4] However, wet chemical analyses do not distinguish between different reduced cations such as Fe^{2+} and Ti^{3+}. Therefore "FeO" possibly includes contributions from both reduced cations
[5] $X_{Fe} = Fe^{2+}/Fe_{total}$

0.03 ($\pm$0.01). Both X_{Fe} are different from those calculated from EM analyses alone (the means are $X_{Fe}=0.14$ and $X_{Fe}=0$, respectively).

Many of the published Mössbauer spectra report different valence state and different site occupancies of Fe (Huggins et al. 1977b; Amthauer et al. 1977; Schwartz et al. 1980; Onuki et al. 1982; Kühberger et al. 1989). The ^{57}Fe *Mössbauer spectrum* of Malenco Ti-andradite reveals resonant absorption peaks mainly of Fe^{3+} and traces of Fe^{2+}. Both doublets are assigned to octahedral ferric and ferrous iron (G. Morin, personal communication), consistent with the results of the site refinements. Because of the low intensitiy of the Fe^{2+} peak it is difficult to fit this doublet exactly. Therefore the "exact" determination of Fe^{2+} contains still some uncertainty. A comparison of the values for Ti-andradite obtained by EM analyses, colorimetry and by Mössbauer spectroscopy, respectively reveals a variation from $X_{Fe}=0.05$ to 0.14. Both colorimetry and Mössbauer spectroscopy data were used to calculate the final garnet formula (see below).

Exchange vectors

The chemical composition of andradite may be expressed in terms of one additive component (andradite $Ca_3Fe_2Si_3O_{12}$) and several exchange vectors. The dodecahedral site is completely occupied by Ca (Table 3). The Si deficiency at the tetrahedral site of the andradite can be explained *completely* and, the Si deficiency in Ti-andradite *partly* by the hydrogarnet substitution (O_4H_4) $(SiO_4)_{-1}$ (Table 5). This is the usual way to incorporate H_2O, as shown for many garnets (mainly grossular-hydrogrossular series, e.g., Lager et al. 1987), and for Ti-andradite by Onuki et al. (1982) and Lager et al. (1989). In contrast, Kühberger et al. (1989) analyzing their synthetic Ti-andradite by FTIR, proposed anion substitution of $(OH)^-$ for O^{2-} in the presence of tetrahedral Fe^{2+}. Regarding the results of the site refinements, there is no evidence for the latter substitution. Besides the hydrogarnet substitution, and according to the results of the site refinements and Mössbauer spectroscopy, most likely small amounts of Al replace Si. This is consistent with the relative preference for substitution on the tetrahedral site given by Huggins et al. (1977a). Therefore Al is accommodated in the tetrahedral site in Val Malenco Ti-andradite suggesting the substitution $Ti^{4+}Al^{IV}$ $(Al^{VI}Si)_{-1}$.

The crystal chemical formula and the exchange vectors were calculated on the basis of 8 cations and 24 positive charges. In order to combine Mössbauer spectroscopy, IR spectroscopy and site refinement data with EM analyses, means of EM data of sample SA 10 (94 and 35 single spot analyses, respectively) were calculated (Table 5). Based on these constraints and considering the two different determinations of ferrous iron, two formulas were calculated for the Ti-rich variety (Table 5). The formula calculation results in significant amounts of Ti^{3+} and can be summarized as follows:

Taking into account that the tetrahedral site is completely occupied by Si and small amounts of hydrogarnet component, the operative Ti-exchange vector for andradite is $Me^{2+}Ti^{4+}$ $2Fe^{3+}_{-1}$. Both formula calculations for Ti-andradite, either based on colorimetry or based on Mössbauer spectroscopy, indicate that substantial amounts of Ti^{3+} are present. However, the calculation using Mössbauer spectra exhibits higher amounts of Ti^{3+} as more Fe is ferric. The incorporation of Ti is therefore best explained by the exchange vectors $Ti^{3+}Fe^{3+}_{-1}$, $Ti^{4+}Al^{IV}$ $(Al^{VI}Si)_{-1}$) and $Me^{2+}Ti^{4+}$ $2Fe^{3+}_{-1}$ (Table 5).

The existence of Ti^{3+} in minerals is a matter of debate. Direct evidence of Ti^{3+} is given by EPR spectroscopy of synthetic minerals (Schneider and Rager 1984; Rager et al. 1993; Löffler et al. 1993). De Groot et al. (1992), investigating a series of natural Ti-minerals by 2p X-ray absorption spectroscopy did not observe Ti^{3+}, except possibly in a Ti-rich andradite garnet. For ligand field reasons and from the studies cited above, Ti^{3+} occupies the octahedral sites.

Ti^{3+} in Ti-andradite is commonly suggested to occur in small concentrations. However, Ti-andradite in ultramafic rocks is often reported to contain significant amounts of Ti^{3+} (Manning and Harris 1970; Huggins et al. 1977b; Schwartz et al. 1980; Onuki et al. 1981, 1982). Kühberger et al. (1989) investigated the crystal chemistry of Ti-andradite synthesized at different oxygen fugacities. Their sample TA 3 synthesized at solid state Ni–NiO exhibits Ti^{3+} together with Ti^{4+} and Fe^{3+} but no Fe^{2+}. In contrast, their sample TA 13 synthesized at iron-quartz-fayalite (IQF) oxygen buffer contains Fe^{2+} and Ti^{3+} together with Fe^{3+} and Ti^{4+}. Virgo et al. (1976) measured a low intrinsic oxygen fugacity in a Ti-andradite from San Benito, California, approximately 4 log units below quartz-fayalite-magnetite (QFM). Furthermore, Peretti et al. (1992) in a study of the Malenco ultramafics calculated the $\log f_{O_2}$ to approximately 4 log units below QFM using the equilibria heazlewoodite + awaruite + magnetite. Peretti et al. (1992) also determined H_2 in fluid inclusions from metamorphic diopside. These conditions may represent the lower limit of $\log f_{O_2}$ as magnetite is a stable member of the paragenesis Ti-andradite + chlorite + diopside. In a similar occurrence of Ti-andradite in San Benito, California, Ti-andradite contains CH_4 in fluid inclusions (M. Van Baalen, personal communication). The presence of reduced Ti^{3+} and small amounts of Fe^{2+} together with Fe^{3+} and Ti^{4+} at similar sites in Val Malenco Ti-andradite may reflect a low oxygen fugacity during crystallisation. The limits of $\log f_{O_2}$ for the Val Malenco Ti-andradite may be given by the above mentioned conditions, e.g, between QFM and 4 log units below QFM.

Composition of chlorite

Chlorite from the samples studied may be described by the general formula $(Mg_{6-x}Al_x)(Si_{4-x}Al_x)O_{10}(OH)_8$, where X is the Al-Tschermaks content of chlorite (Jenkins and Chernosky 1986). From the EM analyses (Table 6) it is evident that the Malenco chlorites have totals reflective of ideal stoichiometry (deviation is less than

Table 6. Representative microprobe analysis of Val Malenco chlorite (1–4, chlorite of the vein paragenesis of sample SA 10; 5, 6, chlorite coexisting with antigorite of sample S 60 for comparison)

Wt%	Sample SA 10				S 60		Average relative error (2σ) in %
	Analysis						
	1	2	3	4	5	6	
SiO_2	30.3	30.7	30.8	30.4	32.9	32.6	0.8
Cr_2O_3	<0.06	<0.06	0.38	0.44	0.65	0.60	15.8 (at 0.5% level)
Al_2O_3	18.8	17.7	17.0	16.9	13.3	13.2	0.8
FeO[1]	9.43	7.62	6.41	6.55	4.49	4.31	3.0
MnO	0.17	0.13	0.06	<0.06	<0.06	<0.06	16.6
MgO	28.3	30.8	32.1	32.0	34.7	35.4	0.6
NiO	0.29	<0.28	<0.28	<0.28	<0.28	<0.28	32.0
H_2O_{calc}	12.34	12.50	12.55	12.46	12.54	12.62	
$\sum$	99.6	99.5	99.3	98.7	98.6	99.1	
Ions calculated on the basis of 10 cations and stoichiometric OH							
Si	2.94	2.95	2.95	2.92	3.14	3.10	
Al^{IV}	1.06	1.05	1.05	1.08	0.86	0.90	
Al^{VI}	1.09	0.96	0.87	0.84	0.64	0.58	
Cr	0.00	0.00	0.03	0.03	0.05	0.05	
Fe^{2+}	0.77	0.61	0.55	0.52	0.36	0.34	
Mn	0.01	0.01	0.01	0.00	0.00	0.00	
Mg	4.10	4.41	4.58	4.59	4.94	5.02	
Ni	0.02	0.00	0.00	0.00	0.00	0.00	
OH	8.00	8.00	8.00	8.00	8.00	8.00	

H_2O_{calc} = stoichometric OH converted into wt% H_2O; TiO_2 < 0.03 wt%
[1] Total Fe as FeO

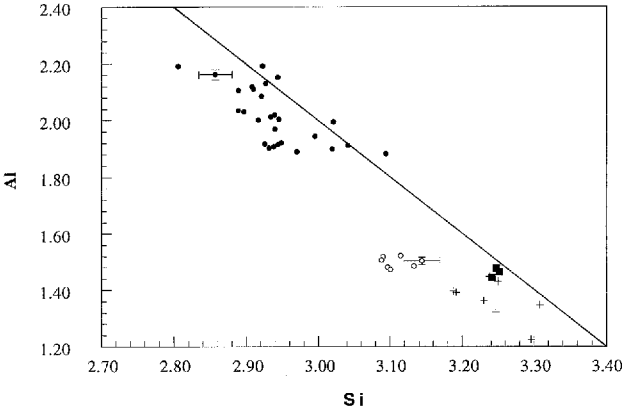

Fig. 8. Si against Al in chlorite from Val Malenco. Idcal clinochlore has Si = 3 and Al = 2 cations per formula unit. Slope of the theoretical line of Al-Tschermak exchange is −1. Deviations below the theoretical line indicate substantial amounts of Fe^{3+}. Note that chlorites from the clinopyroxenite layer, *full dots*, have X values between 0.94 and 1.1. Error *bars* represent the relative error due to counting statistics (2σ). *Open circles*, chlorites of an olivine websterite; *full squares*, chlorites coexisting with antigorite; *crosses*, data from Peretti (1988)

1.5%). Wavelength spectra did not show detectable quantities of Zn, V, K, Ca, Na, Cl and F. The analyzed chlorites contain minor amounts of MnO, NiO and Cr_2O_3 whereas the concentration of TiO_2 is below 0.03 wt% (Table 6). Chlorite coexisting with Ti-andradite and diopside exhibits significantly higher contents of iron than chlorite from antigorite serpentinite.

In Fig. 8 Si is plotted against Al showing that almost all the chlorites are below the theoretical line for the pure Al_2^{3+} $Mg_{-1}Si_{-1}$ exchange. The chlorites show significant differences in their composition which are consistent with optical observations. Chlorite (clinochlore) with $0.95 < X < 1.1$ occurs only in antigorite-free rocks of olivine websterite and clinopyroxenite composition, whereas chlorite (Fe-pennine) with $0.7 < X < 0.8$ coexists with antigorite. *Ti-andradite* is always associated with *clinochlore*.

Mass balance and field observations: a comparison

Mass balance calculations have shown that the paragenesis Ti-andradite + clinochlore + diopside ± magnetite originates without introduction of elements. This is consistent with field observations as no reaction zone is recognizable along the contact with antigorite-rich rocks. The composition of the harzburgitic (A) and lherzolitic (B) rocks results in coexisting, metamorphic chlorite and antigorite (Table 2). Under the given metamorphic conditions (see above) chlorite in equilibrium with antigorite shows a compositional range of $0.65 < X_{Al} < 0.8$ (Fig. 8) which seems to be close to the low-Al composition limit of chlorite (Foster 1962; Peretti 1988). The composition of the normative websteritic (C) and clinopyroxenitic (D) rocks results in an antigorite-free paragenesis containing chlorite with a composition of $X_{Al} = 1.1$. The calculated value is consistent with EM analyses ($0.95 < X_{Al} < 1.1$, Fig. 8).

It is noteworthy that no Ti-andradite and vesuvianite was found in antigorite-rich rocks (A, B). The occurrence of Ti-andradite is restricted to antigorite-free rocks (C, D) with chlorite of $0.95 < X_{Al} < 1.1$. A comparison

between the normative and the metamorphic phase assemblage of rock A–D (mass balance) has shown that the formation of Ti-andradite is likely in rock C and D, but unlikely in rock A and B, consistent with field observations.

Discussion and conclusions

The study of a chlorite clinopyroxenite representing a former igneous layer has shown that Ti-andradite is a stable member of the paragenesis chlorite + diopside + magnetite[6] (± vesuvianite ± perovskite). Ti-andradite does not occur together with serpentine. The conditions of the regional Alpine metamorphism found in that area (400–450° C, Mellini et al. 1987; 4–7 kbar, Guntli and Liniger 1989) constrain the upper limit of formation of the Ti-andradite. These data, especially the formation temperature, are in good agreement with the results of Onuki et al. (1982) and Van Baalen (1991).

The Ti-minerals ilmenite, Ti-andradite and perovskite in the Malenco serpentinite are always associated with diopside and chlorite and are most abundant in virtually monomineralic diopside layers (pyroxenite, Table 2). Some of the primary pyroxenes show perovskite or Ti-andradite as alteration products of former opx and FeTi-oxides (Figs. 3, 4). These observations suggest that magmatic Ti-augites are the source of Ti, similar to occurrences of titanian hydroxyl-clinohumite in the Malenco ultramafics (Trommsdorff and Evans 1980).

The formation of Ti-andradite in veins provides evidence for the mobility of Ti and other elements in an aqueous hydrothermal fluid. The X_{CO_2} of the fluid present during Alpine metamorphism was very low because of the stable paragenesis antigorite + diopside in the surrounding serpentinites ($X_{CO_2} < 0.005$, Trommsdorff and Evans 1977; Trommsdorff and Connolly 1990). This is supported by field observations as no carbonates were found. Only small amounts of species other than H_2O in the fluid phase are observed (Peretti et al. 1992). Titanium transport is reported to occur under a wide variety of conditions, often at higher temperatures and in other geological environments (i.e., skarn deposits, granite alteration zones, basalt alteration zones, chloritic blackwalls), in which F^-, PO_4^{3-}, CO_3^{2-}, and OH^- seem to be the most likely ligands for complexing Ti (Alderton et al. 1980; Hynes 1980; Gieré 1986). The concentration of Ti in geological fluids is limited by the solubility of Ti-oxides; depending on Eh-pH values, temperature and chemical species (Ayers and Watson 1993; Van Baalen 1993; and quoted references). From experimental investigations, the solubility of Ti-oxides is enhanced by fluoride complexes (Barsukova et al. 1979; Bright and Readey 1987), whereas sulfate, carbonate and chloride complexes are not of major importance (Van Baalen 1993 and quoted references).

From the Malenco ultramafics, Ti transport is mostly known from titanian hydroxyl-clinohumite bearing veins which often contain hydroxyl-apatite and perovskite (Trommsdorff and Evans 1980). In contrast, there is no evidence for F^-, CO_3^{2-} and PO_4^{3-}-bearing minerals in the clinopyroxenite, thus indicating that OH^- most likely is an agent complexing Ti. Under moderate to low P, T conditions in ultramafic rocks, aqueous rich fluids may be able to transport Ti on a meter scale.

Taking into account that the dodecahedral site is completely occupied by Ca, the compositional variation in Malenco andradite is consistent with the following exchange vectors:

1. In andradite the tetrahedral site is occupied by Si and small amounts of the hydrogarnet exchange vector $(O_4H_4)\ (SiO_4)_{-1}$. The variation on the octahedral site is attributed to the exchange $AlFe_{-1}$, $CrFe_{-1}$ and $Me^{2+}Ti^{4+}\ 2Fe^{3+}_{-1}$.
2. In Ti-andradite the Si deficiency can be explained by the exchange $(O_4H_4)\ (SiO_4)_{-1}$ and $Ti^{4+}Al^{IV}\ (Al^{VI}Si)_{-1}$ respectively. The variation on the octahedral site is mainly attributed to the Ti exchange vectors $Ti^{3+}Fe^{3+}_{-1}$, $Ti^{4+}Al^{IV}\ (Al^{VI}Si)_{-1}$ and $Me^{2+}Ti^{4+}\ 2Fe^{3+}_{-1}$. Minor exchange vectors are $AlFe_{-1}$, and $CrFe_{-1}$.

Under the given metamorphic conditions and within the analyzed range no compositional gap could be found.

Mass balances have shown that the vein paragenesis Ti-andradite, andradite, chlorite, diopside, magnetite and vesuvianite originates without introduction of elements from the surrounding serpentinite. In the studied ultramafics Ti-andradite and vesuvianite originate *only* in association with chlorite with high Al ($0.95 < X_{Al} < 1.1$). The Al-content of this chlorite differs from antigorite-chlorite paragenesis ($X_{Al} \sim 0.7$). Antigorite-free clinopyroxenites containing clinochlore have most probably formed from an orthopyroxene/olivine poor and clinopyroxene rich layer. Clinopyroxenite rocks of this type are rare in the Malenco ultramafics. Compared to other layers, the chemistry in this layer may be unusual. As reducing conditions seem to be common in the Malenco ultramafics (Peretti et al. 1992), the formation of Ti-andradite may be related to low oxygen fugacity.

Acknowledgements. The authors would like to thank Dr. J.A.D. Connolly (ETH Zürich), Prof. V. Trommsdorff (ETH Zürich), Dr. R. Gieré (Universität Basel), Prof. B.W. Evans (University of Washington) and an anonymous reviewer for their critical and careful reviews of the manuscript. We also express our sincere gratitude to Dr. E. Reusser for assistance at the microprobe. We are specially endebted to M. Leona and M. Merli (Università di Pavia) for undertaking site refinements, G. Morin (Université de Paris) für Mössbauer spectroscopy, H. Hürlimann (Universität Basel) for undertaking IR spectroscopy and to J.C. Lavanchy (Université de Lausanne) for analyzing FeO. The financial support of the Schweizerischer Nationalfonds (No. 20-30768.91 and 2000-037388.93/1) is gratefully acknowledged.

[6] A similar occurrence of the paragenesis Ti-andradite, diopside and chlorite has been reported from the New Idria area, California. The overall compositional range of Ti-andradite, diopside and chlorite is similar, with some tendency for the New Idria chlorites to be more Fe-rich (M. Van Baalen, personal communication)

References

Alderton DHM, Pearce JA, Potts PJ (1980) Rare earth element mobility during granite alteration: evidence from south-west England. Earth Planet Sci Lett 49:149–165

Allen FM, Buseck PR (1988) XRD, FTIR and TEM studies of optically anisotropic grossular garnets. Am Mineral 73:568–584

Amthauer G, Kurtz W, Rost F, Schloemer H (1974) Chemismus and Genese des Andradits aus dem Serpentinit des Val Malenco (Bernina Gebiet, Oberitalien). Schweiz Mineral Petrogr Mitt 54:691–706

Amthauer G, Annersten H, Hafner SS (1977) The Mössbauer spectrum of ^{57}Fe in titanium bearing andradites. Phys Chem Miner 1:399–413

Armbruster T, Geiger CA (1993) Andradite crystal chemistry, dynamic X-site disorder and structural strain in silicate garnets. Eur J Mineral 5:59–71

Ayers JC, Watson EB (1993): Rutile solubility and mobility in supercritical aqueous fluids. Contrib Mineral Petrol 114:321–330

Barsukova ML, Kuznetsov VA, Dorofeyeva VA, Khodakowskiy LI (1979) Measurements of the solubility of rutile TiO_2 in fluoride solutions at elevated pressures. Geochem Int 7:41–49

Basso R, Della Giusta A, Zefiro L (1981) A crystal chemical study of a Ti-containing hydrogarnet. Neues Jahrb Mineral Monatsh:230–236

Bedognè F, Montrasio A, Sciesa E (1993) I minerali della Provincia di Sondrio: Valmalenco. Bettini, Sondrio 1993

Benetti F (1987) I minerali rinvenuti nella zona nord-ovest della Valmalenco comprendente la Bocchetta delle Forbici, la Forcella di Fellaria, il Sasso Moro e la Vedretta orientale di Fellaria con particolare riferimento a quelli tipici delle Rodingiti. Atti ufficiali del convegno Special Publication Val Malenco Natura 1:40–46

Bright E, Readey DW (1987) Dissolution kinetics of TiO_2 in HF-HCl solutions. J Am Ceramic Soc 70:900–906

Bucher K, Pfeifer HR (1973) Über Metamorphose und Deformation der östlichen Malenco-Ultramafitite und deren Rahmengesteine. Schweiz Mineral Petrogr Mitt 53:231–241

Deer WA, Howie RA, Zussman J (1982) Rock-forming minerals, 2nd edn, vol. 1A: orthosilicates. Longman, London

De Groot FMF, Figueiredo MO, Basto MJ, Abbate M, Petersen H, Fuggle JC (1992) 2p X-ray absorption of titanium in minerals. Phys Chem Miner 19:140–147

Dietrich V, Oberhänsli R, Walpen P (1976) Röntgenfluoreszenzanalyse der Silikatgesteine (internal rep). Inst Kristallogr Petrogr ETH Zürich

Dowty E (1971) Crystal chemistry of titanium and zirconian garnet. I. Review and spectral studies. Am Mineral 54:1139–1150

Evans BW, Trommsdorff V, Richter W (1979) Petrology of an eclogite-metarodingite suite at Cima di Gagnone, Ticino, Switzerland, Am Mineral 64:15–31

Evans BW, Trommsdorff V, Goles GG (1981) Geochemistry of high-grade eclogites and metarodingites from the central alps. Contrib Mineral Petrol 76:301–311

Flohr MJK, Ross M (1989) Alkaline igneous rocks of Magnet Cove, Arkansas: metasomatized ijolite xenoliths from Diamond Jo quarry. Am Mineral 74:113–131

Foster MD (1962) Interpretation of the composition and a classification of the chlorites. U.S. Geol Surv Prof Pap 414-A:1–33

Gieré R (1986) Zirconolite, allanite and hoegbomite in a marble skarn from the Bergell contact aureole: implications for mobility of Zi, Zr and REE. Contrib Mineral Petrol 93:459–470

Grammacioli CM (1962) I minerali valtellinesi nella raccoltà di Pietro Sigismund Ed. privata, Milano

Grammacioli CM (1975) Minerali alpini e prealpini. Atlas, Bergamo

Guntli P, Liniger M (1989) Metamorphose in der Margna-Decke im Bereich Piz da la Margna and Piz Fedoz (Oberengadin). Schweiz Mineral Petrogr Mitt 69:289–301

Hermann J (1991) Geologische Untersuchungen südlich der Berninagruppe. I. Diploma thesis, ETH Zürich

Hermann J, Müntener O (1992) Strukturelle Entwicklung im Grenzbereich des penninischen Malenco-Ultramafitits und der unterostalpinen Decken (Margna und Sella). Schweiz Mineral Petrogr Mitt 72:225–240

Honegger K (1977) Der Malencoserpentinit und seine Rahmengesteine östlich der Kette Pizzo Cassandra-Pizzo Rachele. Diploma thesis, ETH Zürich

Howie RA, Woolley AR (1968) The role of titanium and the effect of TiO_2 on the cell size, refractive index and specific gravity in the andradite – melanite – schorlomite series. Mineral Mag 36:775–790

Huggins FE, Virgo D, Huckenholz G (1977a) Titanium containing silicate garnets. I. The distribution of Al, Fe^{3+} and Ti^{4+} between octahedral and tetrahedral sites. Am Mineral 62:475–490

Huggins FE, Virgo D, Huckenholz G (1977b) Titanium containing silicate garnets. II. The crystal chemistry of melanites and schorlomites. Am Mineral 62:646–665

Hynes A (1980) Carbonization and mobility of Ti, Y, and Zr in Ascot Formation Metabasalts, SE Quebec. Contrib Mineral Petrol 75:79–87

Isaacs T (1968) Titanium substitution in andradites. Chem Geol 3:219

Jamtveit B (1991) Oscillatory zonation patterns in hydrothermal grossular-andradite garnet: nonlinear dynamics in regions of immiscibility. Am Mineral 76:1319–1327

Jenkins DM, Chernosky JV (1986) Phase equilibria and crystallochemical properties of Mg-chlorites. Am Mineral 71:924–936

Keusen HR (1972) Mineralogie und Petrographie des metamorphen Ultramafitit-Komplexes vom Geisspfad (Penninische Alpen). Schweiz Mineral Petrogr Mitt 52:385–478

Kingma KJ, Downs JW (1989) Crystal-structure analysis of a birefringent andradite. Am Mineral 74:1307–1316

Kitamura K, Iyi N, Kimura S, Chevrier F, Devignes JM, Le Gall H (1986) Growth-induced optical anisotropy of epitaxial garnet films on (110)-oriented substrates. J Appl Phys 60:1486–1489

Kühberger A, Fehr T, Huckenholz HG, Amthauer G (1989) Chrystal chemistry of a natural schorlomite and Ti-andradites synthesized at different oxygen fugacitites. Phys Chem Miner 16:734–740

Lager GA, Armbruster T, Faber J (1987) Neutron and X-ray diffraction study of hydrogarnet $Ca_3Al_2(O_4H_4)_3$. Am Mineral 72:758–767

Lager GA, Armbruster T, Rotella FJ, Rossman GR (1989) OH-substitution in garnets: X-ray and neutron diffraction, infrared and geometric modelling studies. Am Mineral 74:840–851

Löffler U, Rager H, Bakhshandeh A (1993) Ti^{3+} EPR spectroscopy of synthetic garnets and clinopyroxenes. Terra Abst 1:501

Manning PG (1975) Charge transfer processes and the origin of color and pleochroism of some Ti-rich vesuvianites: evidence for ferric iron in eight coordination. Can Mineral 13:110–116

Manning PG, Harris DC (1970) Optical-absorption and electron-microprobe studies of some high-Ti andradites. Can Mineral 10:260–271

Manning PG, Tricker MJ (1975) Optical absorption and Mössbauer spectral studies of iron titanium site populations in vesuvianite. Can Mineral 13:259–265

Mellini M, Trommsdorff V, Compagnoni R (1987) Antigorite polysomatism: behaviour during progressive metamorphism. Contrib Mineral Petrol 97:147–155

Montrasio A (1984) The "Lanzada-Scermendone Zone": an ophiolitic unit of continental affinity in the southern Rhaetic Alps (Prov. Sondrio-Italy). Schweiz Mineral Petrogr Mitt 66:466–472

Müntener O (1991) Geologische Untersuchungen südlich der Berninagruppe. II. Diploma thesis, ETH Zürich

Murdoch J, Ingram BL (1966) A cerian vesuvianite from California. Am Mineral 51:381–387

Myasnikov VS (1940) On titaniferous vesuvianite from the Perovskite and Akhmat mines of the south Ural. Dokl Acad Sci USSR 28:446–449

Nisbet EG, Dietrich VJ, Esenwein A (1979) Routine trace element determination in silicate minerals and rocks by X-ray fluorescence. Fortschr Mineral 57:264–279

Onuki H, Takeyoshi Y, Nedachi M (1981) Electron probe study of Ti-rich hydroandradites in the Sanbagawa metamorphic rocks. J Jpn Assoc Mineral Petrol Econ Geol 76:239–247

Onuki H, Akasaka M, Takeyoshi Y, Nedachi M (1982) Ti-rich hydroandradite from the Sanbagawa Metamorphic rocks of the Shibukawa Area, Central Japan. Contrib Mineral Petrol 80:183–188

Peretti A (1988) Occurence and stabilities of opaque minerals in the Malenco serpentinite (Sondrio, Northern Italy). Diss, ETH Zürich

Peretti A, Dubessy J, Mullis J, Frost BR, Trommsdorff V (1992) Highly reducing conditions during Alpine metamorphism of the Malenco peridotite (Sondrio, Northern Italy) indicated by mineral paragenesis and H_2 in fluid inclusions. Contrib Mineral Petrol 112:329–340

Pouchon JL, Pichoir F (1984) Un nouveau modèle de calcul pour la microanalyse quantitative par spectrométrie de rayons X. I. Application à l'analyse d'échantillons homogènes. Rech Aerosp 1984–3:167–192

Rager H, Schneider H, Bakhshandeh A (1993) Ti^{3+} centres in mullite. Eur J Mineral 5:511–514

Rice JM (1983) Metamorphism of rodingites. I. Phase relations in a portion of the system $CaO-MgO-Al_2O_3-SiO_2-CO_2-H_2O$. Am J Sci 283:121–150

Sawaki T (1988) Melanite and fassaite from the contact aureole around the Nogo, Hakusan granodiorite body, Central Japan. J Mineral Petrol Econ Geol 83:375–383

Schmidt MW (1989) Petrography and structural evolution of ophiolitic remnants in the Bellinzona Zone, Southern Steep Belt, Central Alps. Schweiz Mineral Petrogr Mitt 69:393–405

Schneider H, Rager H (1984) Occurrence of Ti^{3+} and Fe^{2+} in mullite. Com Am Ceram Soc C248–C250

Schwartz KB, Nolet DA, Burns RG (1980) Mössbauer spectroscopy and crystal chemistry of natural Fe–Ti garnets. Am Mineral 65:142–153

Shibata T, Thompson G (1986) Peridotites from Mid-Atlantic Ridge at 42°N and their petrogenetic relation to abyssal tholeiites. Contrib Mineral Petrol 93:144–159

Sigismund P (1948) Granato e Vesuvianite di Val Malenco. Atti Soc Ital Sci Nat Milano 87

Spillmann P (1993) Die Geologie des penninisch-ostalpinen Grenzbereichs im südlichen Berninagebirge. Diss, ETH Zürich

Switzer G, Melson WG, Thompson G (1970) Garnet from Mid-Atlantic Ridge near 42°N. latitude. Geol Soc Am Bull 81:895–898

Takéuchi Y, Haga N, Umizu S, Sato G (1982) The derivative structures of silicate garnets in grandite. Z Kristallogr 158:53–99

Trommsdorff V, Connolly JAD (1990) Constraints on phase diagram topology for the system $CaO-MgO-SiO_2-H_2O-CO_2$. Contrib Mineral Petrol 104:1–7

Trommsdorff V, Evans BW (1974) Alpine metamorphism of peridotitic rocks. Schweiz Mineral Petrogr Mitt 54:333–352

Trommsdorff V, Evans BW (1977) Antigorite ophicarbonates: phase relations in a portion of the system $CaO-MgO-SiO_2-H_2O-CO_2$. Contrib Mineral Petrol 60:39–56

Trommsdorff V, Evans BW (1980) Titanian hydroxyl-clinohumite: formation and breakdown in antigorite rocks (Malenco, Italy). Contrib Mineral Petrol 72:229–242

Van Baalen MR (1991) A fluid inclusion study of garnets from New Idria, California, USA: new evidence for titanium mobility in aqueous fluids. Plinius 5:235

Van Baalen MR (1993) Titanium mobility in metamorphic systems: a review. Chem Geol (in press)

Virgo D, Rosenhauer M, Huggins FE (1976) Intrinsic oxygen fugacities of natural melanites and schorlomites and crystal-chemical implications. Carnegie Inst Washington Yearb 75:720–729

Weber HP, Virgo D, Huggins FE (1975) A neutron-diffraction and ^{57}Fe Mössbauer study of synthetic Ti-rich garnet. Carnegie Inst Washington Yearb 74:575–577

Zedlitz O (1933) Lime-iron garnets rich in titanium. Zentralbl Mineral Geol A:225–239

Editorial responsibility: J. Hoefs